Electronic orders and phase transitions in a honeycomb Kondo lattice system

Ye Liu[1] and Qiang-Hua Wang[1,2,*]

[1]*National Laboratory of Solid State Microstructures and School of Physics, Nanjing University, Nanjing 210093, China*

[2]*Collaborative Innovation Center of Advanced Microstructures, Nanjing University, Nanjing 210093, China*

(Received 29 June 2017; revised manuscript received 10 August 2017; published 23 August 2017)

We study the electronic orders in a honeycomb-Kondo lattice. For the ground state, we use variational quantum Monte Carlo to find the transition from antiferromagnetic insulator to Kondo insulator is continuous, in contrast to the discontinuous transition in mean-field theory. Moreover, the hybridization parameter between the conduction electron and the Kondo spin is nonzero even within the antiferromagnetic phase. At finite temperatures, we resort to dynamical mean-field theory, which not only captures local quantum fluctuations but also accesses the thermodynamic limit directly. There are three phases, namely, antiferromagnetic insulator, Kondo insulator, and paramagnetic phase. The transition from antiferromagnetic phase to paramagnetic phase is likely discontinuous, while that from antiferromagnetic phase to Kondo insulator phase remains to be continuous at finite temperatures. There is a crossover from the paramagnetic phase, where spin excitations are gapless, to the Kondo insulator phase, where spin excitations are gapped. Our results indicate a significant effect of fluctuations beyond mean-field theory in the honeycomb-Kondo lattice. Since the transition from the antiferromagnetic phase to the Kondo insulating phase occurs at a sizable Kondo coupling, where the Kondo lattice model is inequivalent to the Anderson lattice model, our results are complementary to that for a honeycomb-Anderson lattice.

DOI: 10.1103/PhysRevB.96.075147

I. INTRODUCTION

Heavy fermion materials are a class of transition-metal materials, discovered by Graebner and Ott in 1975 [1]. In such materials, the effective mass of quasiparticles could be heavier than that of bare electrons by two to three orders of magnitude. Superconductivity was also discovered in heavy-fermion materials, such as $CeCu_2Si_2$ [2]. At high temperatures, heavy-fermion materials are not too different from normal metals, since the local moment, on the f orbitals for example, interact only weakly with the conduction electrons. At low temperatures, however, the local moments tend to form spin singlets with conduction electrons, known as the Kondo singlet, resulting in narrow bands near the Fermi level and a small gap of the order of meV between such bands. When the conduction band is particle-hole symmetric, the Fermi level lies in between the narrow bands, forming an insulator. Such behaviors appear in, for example, $Ce_3Bi_4Pt_3$ and CeNiSn, and was called Kondo insulators (KIs) [3]. SmB_6 is another interesting example [4], and was recently further identified as a topological Kondo insulator [5,6].

Theoretically, there are two types of models under concern. The first is the Anderson lattice model (ALM) [7], describing the itinerant conduction electrons and the periodic coupling to electrons on more localized orbitals and hence subject to strong local Coulomb repulsion. The other is the Kondo lattice model (KLM) [8], which can be derived from the ALM in the strong interaction limit. However, when they are taken independently, the two models are not equivalent in the limit of weak interaction in ALM and strong Kondo coupling in KLM. To understand the experimental results, a phenomenological two-fluid model has also been developed in an attempt to describe the itinerant and localized behaviors of electrons [9,10].

The behaviors of KLM can be roughly understood by the well-known Doniach picture [8,11]. There are two competing effects that determine the ground state of KLM. The first is the Kondo screening that tries to force the local moments and conduction electrons to form spin singlets. The other is the effective coupling between local moments via the conduction electrons, known as the RKKY interaction [12]. The characteristic energy scale for Kondo screening is just the Kondo temperature $T_K \sim De^{-1/2J\rho}$, where D is roughly the conduction bandwidth, J is the antiferromagnetic coupling between local moments and conduction electrons (the Kondo coupling), and ρ is the conduction density of states. On the other hand, the energy scale of RKKY coupling is $J_{RKKY} \sim \chi J^2$, where χ is the spin susceptibility in the conduction band. Therefore, the RKKY coupling dominates for small J, and the system favors a magnetic ordering at a wave vector where χ is largest. In contrast, when J becomes larger, Kondo screening may become dominant and the system favors a nonmagnetic state. Because of the strong coupling between local moments and conduction electrons, the system settles down in a heavy-fermion metallic state if the conduction band is away from particle-hole symmetry, or a KI if the particle-hole symmetry is present.

While the Doniach picture provides qualitative insights, the understanding of KLM is far from complete. The existence of magnetic order and in particular the critical nature of the transition from magnetic to nonmagnetic states are important issues to explore. In the one-dimensional KLM, e.g., it is found that at half filling the KLM is always in an insulating spin-liquid state [13,14]. In two dimensions, the phase diagram is richer but less thoroughly understood. Because of the lack of exact solutions, numerical studies are indispensable, such as quantum Monte Carlo (QMC) [15,16], variational Monte Carlo (VMC) [17–19], series expansion [20], density-matrix renormalization group [21], and dynamical mean-field theory (DMFT) [22,23], etc. The simple Hatree-Fock mean field theory (HFMFT) is also an easy option. Although it is not

*qhwang@nju.edu.cn

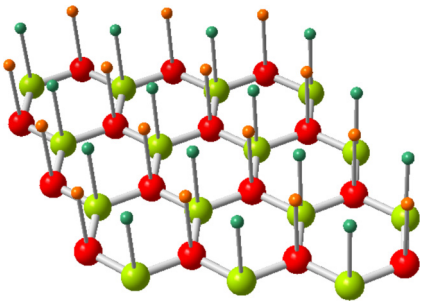

FIG. 1. Illustration of the two-dimensional HKL. The red/blue symbols indicate the A/B sublattice. The conduction electrons move on the bottom layer, while the local moments are on the tops of the vertical bonds.

expected to be reliable in low dimensions, it may indicate correctly the types of possible orders. At or above the upper critical dimension, it should provide qualitatively correct results. For example, mean-field results (at zero temperature) for a three-dimensional KLM [24] appear to be in qualitative agreement with the Doniach picture. Therefore the KLM in two dimensions appears particularly challenging in theory.

The two-dimensional honeycomb lattice is even more special in that the dispersion is linear near the Dirac points. At half filling the Fermi level is at the Dirac points, and the low-energy density of states (DOS) is linear in energy. The recently discovered graphene is in such a structure [25,26], providing a platform to manipulate Dirac fermions in crystal. Here we are interested in the correlation effects. In usual metals, the instability of the normal state is a result of the conspiration of interaction and finite DOS at the fermi level. For example, Kondo screening always happens at sufficiently low temperatures, irrespectively of how small (but nonzero) Kondo coupling is, a consequence of infrared logarithmic divergence. With a linear DOS, infrared logarithmic divergence is expected to be absent, and electronic instabilities may require finite interactions. In fact, it is found that the Kondo spin cannot be screened even down to zero temperature in this case [27]. It is therefore interesting to ask what the interaction would cause if the local moments could be deposited periodically on the lattice, forming a honeycomb-Kondo lattice (HKL). Technically such a lattice can also be cooked up using cold atoms. A schematic plot of HKL is presented in Fig. 1.

Qualitatively, the HKL can also be understood in the Doniach picture. The conduction electrons mediate (Ruderman-Kittel-Kasuya-Yosida (RKKY) interactions at the momentum connecting two Dirac points, which is antiferromagnetic within the unit cell. The RKKY interaction is of the order of $\chi_Q J^2$, where χ_Q is the antiferromagnetic susceptibility of the conduction band, which is finite even though the DOS is linear near the Fermi level. (In a half-filled tight-binding square lattice, the susceptibility is logarithmically divergent.) When an antiferromagnetic order appears, the conduction band is gapped, and the system may be called an antiferromagnetic insulator (AFI). However, the nature of the transition from AFI to KI states has to be investigated more carefully due to the low dimensionality. In a zero-temperature HFMFT in the continuum limit of the HKL [28], it is found that the transition is discontinuous: there is no hybridization between the local moment and the conduction electrons in the AFI phase, but it appears abruptly in the nonmagnetic KI phase. Since the HFMFT ignores quantum fluctuations as well as spatial correlations of fluctuations, all of which are important in low dimensions, investigations beyond HFMFT are necessary. Indeed, finite-temperature quantum Monte Carlo calculations for the honeycomb-Anderson lattice (HAL) show the transition is continuous [29]. (We notice that by the Mermin-Wagner theorem there is no genuine AF order at finite temperatures in two dimensions [30], therefore AF order at finite temperatures henceforth should be understood in the sense of strong AF correlations.) Given the fact that the quantum Monte Carlo is performed at finite temperatures and in finite-sized HKL, and the fact that HKL in the limit of large Kondo coupling and HAL in the limit of weak Hubbard repulsion are not equivalent, here we provide complementary investigations for the HKL.

The main results of this paper are as follows. We perform VMC calculations for the ground state of HKL. We find AFI and KI phases with increasing J, and the transition from AFI to KI is continuous, in contrast to HFMFT. Moreover, the hybridization parameter between the conduction electron and the Kondo spin is nonzero even within the AFI phase. We further perform DMFT calculations at finite temperatures, which not only captures local quantum fluctuations but also accesses the thermodynamic limit directly. The transition from the AFI to the paramagnetic (PM) state is likely discontinuous, while that from AFI to KI remains continuous at finite temperatures. There is a crossover from the gapless PM phase to the gapful KI phase in terms of spin excitation.

The rest of the paper is arranged as follows. In Sec. II, we perform lattice HFMFT for HKL model at zero temperature for self-completeness and comparison. In Sec. III we present VMC results, and in Sec. IV we discuss the DMFT results. We summarize the results in Sec. V.

II. HFMFT FOR HKL

For self-completeness and for comparison to later results, we perform HFMFT for the HKL directly on the lattice. The Hamiltonian is written as

$$H = -t \sum_{\langle ij\rangle\sigma} (c^\dagger_{i\sigma} c_{j\sigma} + \text{H.c.}) + J \sum_i s_i S_i, \tag{1}$$

where t is the hopping on nearest-neighbor bonds, J is the Kondo coupling, $c_{i\sigma}$ annihilates a conduction electron at site i with spin polarity σ, and s_i and S_i are the spin operator for a conduction electron and the f electron on Kondo sites, respectively. The f electron on a Kondo site is subject to single-occupancy constraint,

$$n_{f,i} = \sum_\sigma f^\dagger_{i\sigma} f_{i\sigma} = 1. \tag{2}$$

We set $t = 1$ as the unit of energy henceforth. The honeycomb lattice has two sublattices A (red) and B (green), as illustrated in Fig. 1. In the mean-field ansatz, we assume a hybridization order parameter

$$\xi = \sum_\sigma \langle c^\dagger_{i\sigma} f_{i\sigma} + \text{H.c.}\rangle, \tag{3}$$

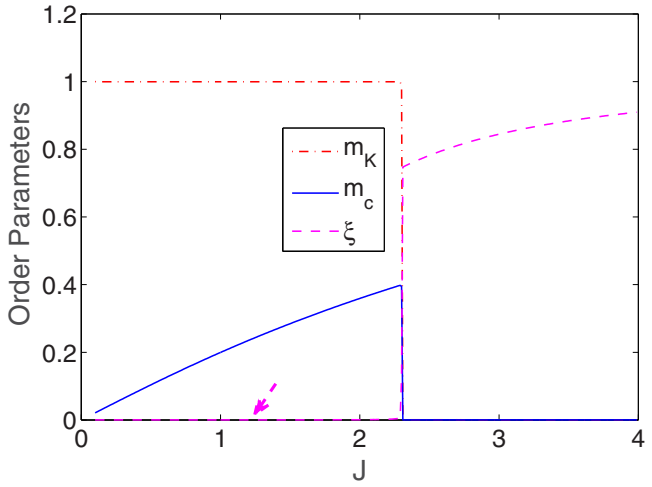

FIG. 2. Mean field order parameters versus the Kondo coupling J. If the magnetic order is suppressed, ξ appears at a smaller J indicated by the arrow.

and magnetic order parameters

$$m_c = 2\eta_i\langle s_i^z\rangle, \quad m_K = -2\eta_i\langle S_i^z\rangle, \tag{4}$$

on the conduction/Kondo site, where $\eta_i = \pm 1$ for sublattice A/B reflecting the antiferromagnetic configuration within a unit cell, and z indicates the z component of the spins. The mean-field Hamiltonian reads

$$H_{MF} = -t\sum_{\langle ij\rangle\sigma}(c_{i\sigma}^\dagger c_{j\sigma} + \text{H.c.}) + \frac{J}{2}\sum_i \eta_i\left(m_c S_i^z - m_K s_i^z\right) - \frac{J\xi}{2}\sum_{i\sigma}(c_{i\sigma}^\dagger f_{i\sigma} + \text{H.c.}), \tag{5}$$

which can be diagonalized easily in momentum space. The order parameters are determined self-consistently using the mean-field Hamiltonian. The single-occupancy constraint for the f electrons is relaxed to average half filling, $\langle n_{f,i}\rangle = 1$. Within the mean-field approximation, it is straightforward to prove that once $\xi \neq 0$ and/or $m_c m_K > 0$ (favorable because of the antiferromagnetic Kondo coupling) the mean-field bands are gapped. Hence such ordered states are insulating. We include the two kinds of orders simultaneously in the calculations, and we optimize the order parameters by minimizing the average energy $E_{MF} = \langle MF|H|MF\rangle$, where H is the original Hamiltonian and $|MF\rangle$ is the mean-field ground state. The average can be obtained by simple Wick contractions.

Figure 2 shows the dependence of the order parameters on the Kondo coupling J. For $J \leqslant 2.27$ the AFI state has lower energy. Here $m_K = 1$, meaning the Kondo spin is fully polarized, while m_c increases monotonically with J. For $J \geqslant 2.27$ the KI state is more favorable, characterized by a finite ξ. As found in Ref. [28], the magnetic ($m_{c,K}$) and hybridization (ξ) order parameters do not appear simultaneously, and the transition from AFI to KI is discontinuous. This is a first-order quantum phase transition. Indeed, we find hysteresis behavior near $J = 2.27$ if we cycle J adiabatically during the self-consistent calculations. Moreover, if we suppress the magnetic order, the hybridization order would emerge already at $J \sim 1.2$, as indicated by the arrow in Fig. 2.

III. VMC FOR HKL

In this section we perform a VMC study of the HKL model. We take the following variational Hamiltonian:

$$H_x = -\sum_{\langle ij\rangle\sigma}(c_{i\sigma}^\dagger c_{j\sigma} + \text{H.c.}) + \sum_i \eta_i\left(\mu_c S_i^z - \mu_K s_i^z\right) - V\sum_{i\sigma}(c_{i\sigma}^\dagger f_{i\sigma} + \text{H.c.}), \tag{6}$$

with variational parameters $x = (\mu_c, \mu_K, V)$. This Hamiltonian determines a Slater-determinant ground state $|G_0(x)\rangle$, which is used in the trial ground state for the original many-body Hamiltonian H:

$$|G(x)\rangle = P|G_0(x)\rangle, \quad P \equiv \Pi_i(1 - e^{i\pi n_{f,i}}), \tag{7}$$

where P projects away from $|G_0(x)\rangle$ any real-space basis components violating single occupancy of the f electrons on the Kondo sites. The variational parameters are optimized by minimizing the energy (per electron),

$$E(x) = \frac{1}{2N}\frac{\langle G(x)|H|G(x)\rangle}{\langle G(x)|G(x)\rangle}, \tag{8}$$

where N is the number of sites for c (or f) electrons. We notice that $\mu_{c,K}$ breaks spin-rotational symmetry as $m_{c,K}$ does in HFMFT. If $V = 0$, the conduction electrons and f electrons are decoupled, and $E(x)$ becomes identical to E_{MF}. However, the two sectors are coupled when $V \neq 0$, and VMC is nontrivial. For example, while V breaks the local U(1) gauge symmetry $f_{i\sigma} \to f_{i\sigma}e^{i\theta_i}$ in $|G_0(x)\rangle$, as ξ does in $|MF\rangle$, this symmetry is restored by the projection operator P in $|G(x)\rangle$. In this sense, VMC equivalently integrates over all quantum gauge fluctuations, and the variational parameter V should be understood as a parameter that organizes the spin-spin correlations in the variational ground state, rather than a gauge-symmetry breaking order. (In fact only the absolute value $|V|$ matters in VMC.) In practice $E(x)$ has to be evaluated by Monte Carlo sampling since the dimension of the many-body Hilbert space increases exponentially with the size of the system. Notice that VMC is controlled statistically but is subject to systematical error if $|G(x)\rangle$ deviates from the exact ground state. For technical details of VMC, see, e.g., Refs. [31–33]. For comparison to HFMFT, we also calculate the average spin moments,

$$m_c = \frac{2}{N}\sum_i \frac{\eta_i\langle G(x)|s_i^z|G(x)\rangle}{\langle G(x)|G(x)\rangle}, \quad m_K = -\frac{2}{N}\sum_i \frac{\eta_i\langle G(x)|S_i^z|G(x)\rangle}{\langle G(x)|G(x)\rangle}. \tag{9}$$

We use these averages to characterize the VMC results, but we work with $\mu_{c,K}$ (and V) in the actual VMC calculations.

In order to benchmark the accuracy of VMC as well as the finite-size effect, we first perform VMC and exact diagonalization (ED) for a small-sized HKL with 2×2 unit cells ($N = 8$). The inset of Fig. 3 shows the variational ground-state energy from VMC (line with error bars) versus

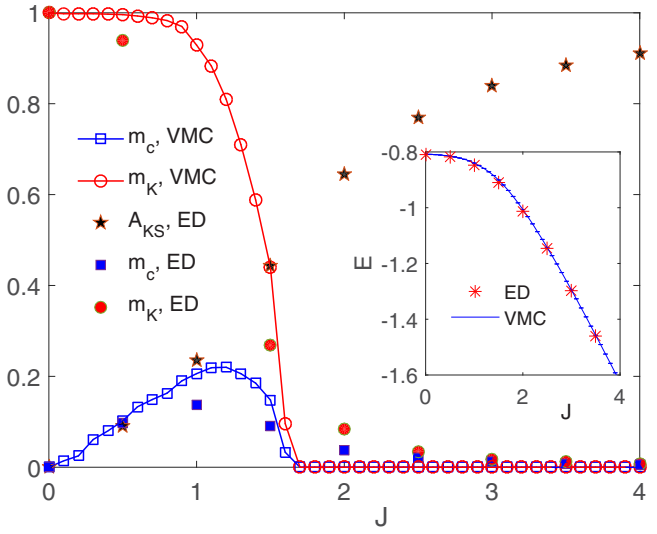

FIG. 3. Results in a HKL with 2×2 unit cells ($N = 8$). Main panel: (m_c, m_K) from VMC (open symbols), and (m_c, m_K, V) and Kondo screening amplitude A_{KS} from exact diagonalization (filled symbols) under a small exchange bias field acting on the Kondo spins. Inset: Ground-state energy E per electron from VMC (line) and exact diagonalization (symbols). See the main text for more details. The statistical error bars in VMC results are well within the symbol size.

J, and the exact ground-state energy by ED (symbols). The agreement between VMC and ED is perfect. In the main panel of Fig. 3, we show (m_c, m_K) from VMC (open symbols). Clearly (m_c, m_K) drops to zero continuously around $J = 1.65$, and on the other hand, V is finite at all finite values of J. For comparison, we also calculate (m_c, m_K) by ED. We find they vanish in the exact ground state of H in the small system. However, if we add to H a small bias $-h \sum_i \eta_i S_i^z$, with $h = 0.01$, spin moments are generated and shown as filled symbols in the main panel. The magnetic response to the bias is strong in the small-J regime, and a crossover to weak or linear response is seen at higher values of J. The crossover point is in agreement with the transition point in the VMC result. We further calculate by ED the amplitude of Kondo screening (KS),

$$A_{KS} = -\frac{4}{3}\langle s_i S_i \rangle, \tag{10}$$

shown as filled stars in the main panel. It increases steadily with increasing J. In the fully screened case it should saturate to unity. We find $A_{KS} \gg -(4/3)\langle s_i^z \rangle \langle S_i^z \rangle = m_c m_K/3$. This is a manifestation of significant correlation of quantum spin fluctuations on top of the ordered moments.

We now present VMC results on a larger HKL with 6×6 unit cells ($N = 72$). The main panel of Fig. 4 shows the optimized energy E versus J when all of the variational parameters are taken into account. For comparison, the inset shows the corresponding energy E_V (or E_m) if only V (or $m_{c,K}$) is included in VMC, with E as the reference. We see that both E_V and E_m are higher than E for $J < 1.7$, suggesting that all variational parameters are nonzero in this regime in order to optimize E. For $J > 1.7$, $E_m > E$ and $E_V = E$, hence magnetic order should be absent in this regime. Figure 5 shows

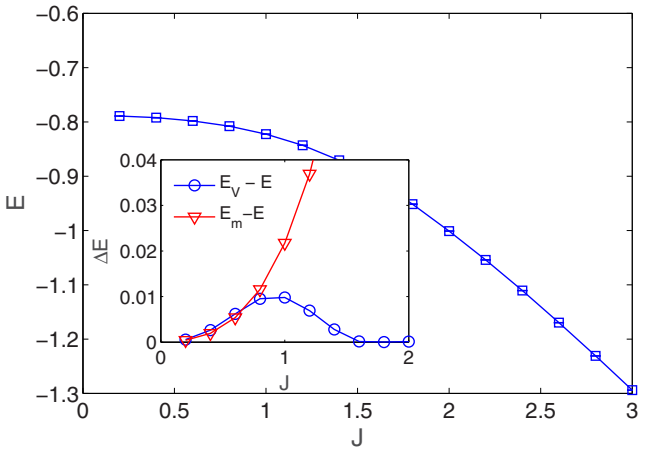

FIG. 4. VMC results for a HKL with 6×6 unit cells. Main panel: optimized average energy E (per electron) with respect to all variational parameters (m_c, m_K, V). For comparison, the inset shows the corresponding optimized energy E_V (or E_m) if only V (or $m_{c,K}$) is taken into account in VMC, with E as the reference. The statistical error bars are well within the symbol size and hence not shown in the inset.

explicitly the order parameters from VMC. With increasing J, m_K decreases monotonically, while m_c increases first and then decreases. Both magnetic moments decrease continuously to zero at $J = 1.7$. This marks the continuous quantum phase transition from AFI to KI. Importantly, V is nonzero even in the AFI phase, suggesting partial Kondo screening coexisting with the magnetic order. The continuous transition as well as the coexistence of partial Kondo screening are qualitatively different from the HFMFT results. In fact, such features are also found in KLM on square lattices [15,16,18,34]. Combining our results for HKL, we conclude they are general features of particle-hole symmetric KLMs. We stress that the overall features in Fig. 5 are consistent with the results in

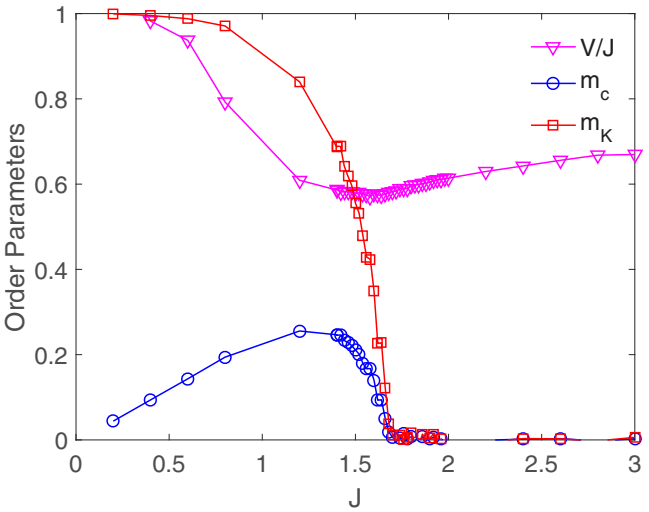

FIG. 5. Order parameters from VMC on a HKL with 6×6 unit cells ($N = 72$). The statistical error bars are well within the symbol size and hence are not shown.

Fig. 3, implying weak finite-size effect. The underlying reason can be traced to the fact that the system is always gapped, satisfying the so-called close-shell condition that is important for the stability of VMC.

IV. DMFT FOR HKL

Finally we perform DMFT for the HKL at finite temperatures. Although DMFT is not exact, since it ignores spatial correlation of fluctuations, it does capture local quantum fluctuations and accesses thermodynamic limit directly. For the HKL, DMFT proceeds as follows. First we assume an effective quantum impurity problem consisting of a conduction site coupled to a Kondo impurity site. We assume the conduction site is described by a bare local Green's function $g_{0\sigma}(i\omega_n)$, characterized by the hybridization function $\Delta_\sigma(i\omega_n)$ via

$$g_{0\sigma}^{-1}(i\omega_n) = i\omega_n + \Delta_\sigma(i\omega_n). \tag{11}$$

Here ω_n is the Matsubara frequency. The coupling to the Kondo site causes a dressed Green's function $g_\sigma(i\omega_n)$ which can be written as

$$g_\sigma^{-1}(i\omega_n) = g_{0\sigma}^{-1} - \Sigma_\sigma(i\omega_n), \tag{12}$$

where $\Sigma_\sigma(i\omega_n)$ is the self-energy. The Green's function $g_\sigma(i\omega_n)$ is obtained by the strong-coupling version of the continuous-time quantum Monte Carlo (CTQMC) [35–37]. By the assumption of antiferromagnetic order on HKL,

$$\begin{aligned} g_{0\sigma}^A(i\omega_n) &= g_{0\bar\sigma}^B(i\omega_n) = g_{0\sigma}(i\omega_n), \\ \Sigma_\sigma^A(i\omega_n) &= \Sigma_{\bar\sigma}^B(i\omega_n) = \Sigma_\sigma(i\omega_n), \end{aligned} \tag{13}$$

where $\bar\sigma = -\sigma$, and A/B indicates the local functions on the A/B sublattice. Thus we only have to solve one impurity problem in practice. Furthermore, by particle-hole symmetry, we have

$$g_{0\downarrow}(i\omega_n) = -g_{0\uparrow}^*(i\omega_n), \quad \Sigma_\downarrow(i\omega_n) = -\Sigma_\uparrow^*(i\omega_n). \tag{14}$$

This can be utilized to improve the statistics further. After $\Sigma_\sigma(i\omega_n)$ is obtained, we obtain the unit-cell-wise local Green's function by the Hilbert transformation,

$$G_\sigma(i\omega_n) = \int \frac{d^2\mathbf{k}}{(2\pi)^2} \begin{pmatrix} i\omega_n - \Sigma_\sigma & X_\mathbf{k} \\ X_\mathbf{k}^* & i\omega_n + \Sigma_\sigma^* \end{pmatrix}^{-1}. \tag{15}$$

Here G is a 2×2 matrix acting on the sublattice basis, the integration is over the reduced Brillouine zone, and $X_\mathbf{k}$ is the tight-binding dispersion of the c electrons. We extract the diagonal element $g_\sigma(i\omega_n) = G_\sigma^{11}(i\omega_n)$ and update $g_{0\sigma}(i\omega_n)$ and $\Delta_\sigma(i\omega_n)$ via

$$g_{0\sigma}^{-1}(i\omega_n) = g_\sigma^{-1}(i\omega_n) + \Sigma_\sigma(i\omega_n) \to i\omega_n + \Delta_\sigma(i\omega_n). \tag{16}$$

The process is iterated until convergence is achieved in $g_\sigma(i\omega_n)$ or $\Delta_\sigma(i\omega_n)$. Since CTQMC uses directly $\Delta_\sigma(\tau)$, the Fourier transformation of $\Delta_\sigma(i\omega_n)$, we end the iteration if the difference between successive $\Delta(\tau)$'s is smaller than 10^{-4}. In the meantime, we obtain the averages $m_c = 2\langle s^z\rangle$ and $m_K = -2\langle S^z\rangle$ on the conduction and Kondo sites, respectively. For technical details on DMFT, see, e.g., Refs. [38–41].

Figure 6(a) shows the DMFT results at the inverse temperature $\beta = 10\pi$. We see $m_{c,K}$ are finite only at finite J and

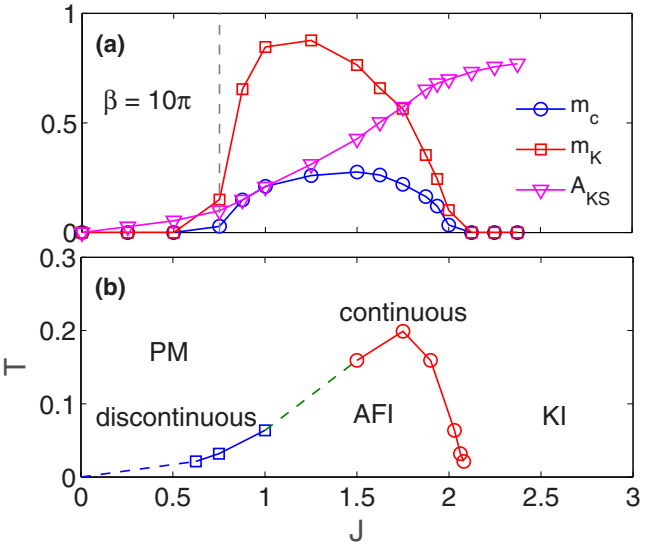

FIG. 6. DMFT results for HKL. (a) $m_{c,K}$ and A_{KS} vs J at the inverse temperature $\beta = 10\pi$. The dashed line highlights the discontinuous transition from PM to AFI phase. (b) Phase diagram in the T-J parameter space. The lines are provided to guide the eye.

below $J = 2.1$. The difference to the case of zero temperature is due to thermal fluctuations. We notice that the convergence of the DMFT iteration is difficult to achieve for smaller J, implying the transition from paramagnetic (PM) state to AFI state is likely first order. However, the convergence is smooth at higher J, and the transition is continuous at $J = 2.1$ where $m_{c,K}$ vanishes continuously. We also calculate A_{KS} in DMFT to have an idea of the extent of Kondo screening. We see that A_{KS} is nonzero for all finite J, and we find it is much higher than the ordered part, $A_{KS} \gg -(4/3)\langle s\rangle\cdot\langle S\rangle = m_c m_K/3$. As in VMC, this implies that there are significant spin fluctuations on top of the average moments (if any), and we also take this as an indication of partial Kondo screening in the AFI phase. By systematic calculations at various temperatures, we end up with a phase diagram shown in Fig. 6(b). The transition between AFI and PM phases is discontinuous (at least for $J \leqslant 1$), while that between KI and PM is continuous. We should point out that the PM phase and the KI phase are not different in symmetry, but the spin excitations are gapped in the KI phase. Hence the transition from PM to KI is just a crossover. Finally we observe that $T \sim J^2$ on the left phase boundary (where J is small). This can be understood from the fact that the energy gain from magnetic ordering is of order J^2, and on the other hand the entropic free-energy gain in the disordered phase is proportional to T. These factors combine to explain the line shape of the left phase boundary qualitatively, and possibly also the discontinuous nature of the phase transition. Since DMFT ignores spatial correlation of fluctuations, the discontinuous transition discussed here deserves further investigations by, e.g., dynamical cluster approximation or QMC. However, we notice that a similar discontinuous transition was pointed out in the QMC result for the HAL model [29], showing that it is unlikely an artefact of DMFT.

V. SUMMARY

We investigated the electronic orders and phase transitions in the HKL model. The HFMFT at zero temperature reveals the AFI and KI states and the discontinuous transition, in qualitative agreement to that in Ref. [28]. VMC calculations show however the transition is continuous, and moreover, the hybridization parameter between the conduction electron and the Kondo spin is nonzero even within the AFI phase. Finally the DMFT calculations at finite temperatures also show the transition between AFI and KI is continuous, and there is a transition from the AFI to PM phase which is likely discontinuous and the phase boundary may be understood in terms of entropic effect. There is a crossover from the gapless PM to gapful KI phase in terms of spin excitations. Since the transition from AFI to KI occurs at a sizable J, where the HKL and HAL are not exactly equivalent, our results are complementary to Ref. [29] for the HAL.

ACKNOWLEDGMENTS

We thank L. Yang for generous help during the VMC calculations. The project was supported by National Key Research and Development Program of China (under Grant No. 2016YFA0300401) and NSFC (under Grant No.11574134).

[1] K. Andres, J. E. Graebner, and H. R. Ott, Phys. Rev. Lett. **35**, 1779 (1975).
[2] F. Steglich, J. Aarts, C. D. Bredl, W. Lieke, D. Meschede, W. Franz, and H. Schäfer, Phys. Rev. Lett. **43**, 1892 (1979).
[3] G. Aeppli and Z. Fisk, Condens. Matter Phys. **16**, 155 (1992).
[4] A. Menth, E. Buehler, and T. H. Geballe, Phys. Rev. Lett. **22**, 295 (1969).
[5] M. Dzero, K. Sun, V. Galitski, and P. Coleman, Phys. Rev. Lett. **104**, 106408 (2010).
[6] R. Yu, H. Weng, X. Hu, Z. Fang, and X. Dai, New J. Phys. **17**, 023012 (2015).
[7] T. M. Rice and K. Ueda, Phys. Rev. Lett. **55**, 995 (1985).
[8] S. Doniach, Physica B + C **91**, 231 (1977).
[9] Y.-F. Yang and D. Pines, Phys. Rev. Lett. **100**, 096404 (2008).
[10] Y.-f. Yang and D. Pines, Proc. Natl. Acad. Sci. USA **109**, E3060 (2012).
[11] P. Coleman, in *Handbook of Magnetism and Advanced Magnetic Materials*, edited by H. Kronmuller and S. Parkin, Vol. 1, Fundamentals and Theory (John Wiley and Sons, 2007), pp. 95–148.
[12] M. A. Ruderman and C. Kittel, Phys. Rev. **96**, 99 (1954).
[13] M. Sigrist, H. Tsunetsugu, K. Ueda, and T. M. Rice, Phys. Rev. B **46**, 13838 (1992).
[14] H. Tsunetsugu, M. Sigrist, and K. Ueda, Rev. Mod. Phys. **69**, 809 (1997).
[15] F. F. Assaad, Phys. Rev. Lett. **83**, 796 (1999).
[16] S. Capponi and F. F. Assaad, Phys. Rev. B **63**, 155114 (2001).
[17] Z. Wang, X.-P. Li, and D.-H. Lee, Physica B: Condens. Matter **199-200**, 463 (1994).
[18] H. Watanabe and M. Ogata, Phys. Rev. Lett. **99**, 136401 (2007).
[19] M. Z. Asadzadeh, F. Becca, and M. Fabrizio, Phys. Rev. B **87**, 205144 (2013).
[20] Z.-P. Shi, R. R. P. Singh, M. P. Gelfand, and Z. Wang, Phys. Rev. B **51**, 15630 (1995).
[21] S. Smerat, U. Schollwöck, I. P. McCulloch, and H. Schoeller, Phys. Rev. B **79**, 235107 (2009).
[22] R. Peters, N. Kawakami, and T. Pruschke, J. Phys.: Conf. Ser. **320**, 012057 (2011).
[23] J. Werner and F. F. Assaad, Phys. Rev. B **88**, 035113 (2013).
[24] C. Lacroix and M. Cyrot, Phys. Rev. B **20**, 1969 (1979).
[25] K. S. Novoselov, A. K. Geim, S. V. Morozov, D. Jiang, Y. Zhang, S. V. Dubonos, I. V. Grigorieva, and A. A. Firsov, Science **306**, 666 (2004).
[26] K. S. Novoselov, A. K. Geim, S. V. Morozov, D. Jiang, M. I. Katsnelson, I. V. Grigorieva, S. V. Dubonos, and A. A. Firsov, Nature (London) **438**, 197 (2005).
[27] L. Fritz and M. Vojta, Rep. Prog. Phys. **76**, 032501 (2013).
[28] Y. Zhong, K. Liu, Y.-F. Wang, Y.-Q. Wang, and H.-G. Luo, Eur. Phys. J. B **86**, 1 (2013).
[29] H.-F. Lin, H.-S. Tao, W.-X. Guo, and W.-M. Liu, Chin. Phys. B **24**, 057101 (2015).
[30] N. D. Mermin and H. Wagner, Phys. Rev. Lett. **17**, 1133 (1966).
[31] H. Yokoyama and H. Shiba, J. Phys. Soc. Jpn. **56**, 1490 (1987).
[32] S. Sorella, Phys. Rev. B **71**, 241103 (2005).
[33] F. Tan and Q.-H. Wang, Phys. Rev. Lett. **100**, 117004 (2008).
[34] G.-M. Zhang and L. Yu, Phys. Rev. B **62**, 76 (2000).
[35] E. Gull, A. J. Millis, A. I. Lichtenstein, A. N. Rubtsov, M. Troyer, and P. Werner, Rev. Mod. Phys. **83**, 349 (2011).
[36] A. N. Rubtsov, V. V. Savkin, and A. I. Lichtenstein, Phys. Rev. B **72**, 035122 (2005).
[37] P. Werner, A. Comanac, L. de' Medici, M. Troyer, and A. J. Millis, Phys. Rev. Lett. **97**, 076405 (2006).
[38] A. Georges, G. Kotliar, W. Krauth, and M. J. Rozenberg, Rev. Mod. Phys. **68**, 13 (1996).
[39] A. Georges and G. Kotliar, Phys. Rev. B **45**, 6479 (1992).
[40] G. Kotliar, S. Y. Savrasov, K. Haule, V. S. Oudovenko, O. Parcollet, and C. A. Marianetti, Rev. Mod. Phys. **78**, 865 (2006).
[41] W. Metzner and D. Vollhardt, Phys. Rev. Lett. **62**, 324 (1989).